MODELLING THE FRACTURE BEHAVIOUR OF ADHESIVELY-BONDED JOINTS AS A FUNCTION OF TEST RATE

A. Karac[1], B. R. K. Blackman[2], V. Cooper[1], A. J. Kinloch[2], S. Rodriguez Sanchez[2], W. S. Teo[2], A. Ivankovic[1]

[1] *School of Electrical, Electronic and Mechanical Engineering, University College Dublin*
[2] *Mechanical Engineering Department, Imperial College London, SW7 2AZ, UK*

Corresponding authors:
E-mail address: alojz.ivankovic@ucd.ie (A. Ivankovic),tel.: +35317161994, fax: +35312830534.
E-mail address: a.kinloch@imperial.ac.uk (A. J. Kinloch), tel.: +442075947000, fax: +442075947238.

ABSTRACT

Tapered-double cantilever-beam joints were manufactured from aluminium-alloy substrates bonded together using a single-part, rubber-toughened, epoxy adhesive. The mode I fracture behaviour of the joints was investigated as a function of loading rate by conducting a series of tests at crosshead speeds ranging from 3.33×10^{-6} m/s to 13.5 m/s. Unstable, (i.e. stick-slip crack) growth behaviour was observed at test rates between 0.1 m/s and 6 m/s, whilst stable crack growth occurred at both lower and higher rates of loading. The adhesive fracture energy, G_{Ic}, was estimated analytically, and the experiments were simulated numerically employing an implicit finite-volume method together with a cohesive-zone model. Good agreement was achieved between the numerical predictions, analytical results and the experimental observations over the entire range of loading rates investigated. The numerical simulations were able very readily to predict the stable crack growth which was observed, at both the slowest and highest rates of loading. However, the unstable crack propagation that was observed could only be predicted accurately when a particular rate-dependent cohesive zone model was used. This crack-velocity dependency of G_{Ic} was also supported by the predictions of an adiabatic thermal-heating model (ATM).

*Keywords:*Adhesive joints; Cohesive-zone model; High-rate; Finite-volume modelling; Fracture mechanics; Rate dependent; Stick-slip.

NOMENCLATURE

a	Crack length
a_0	Initial crack length
a^*	Crack length correction
$\dot{a}$	Average crack velocity
b	Joint width
C_L	Longitudinal wave speed of the substrate material
E_s	Young's modulus of the substrate
E_a	Young's modulus of the adhesive
G_{Ic}	The Mode I adhesive fracture energy
G_{Ic}^s	Static Mode I adhesive fracture energy
h	Adhesive layer thickness

H	Constraint factor
I_s	Moment of inertia of the substrate beam
k	Linear stiffness of the adhesive
m	Geometry factor
L	Length of the beam
P	Load
UTS	Uniaxial tensile strength
V	Test rate
v_x	Displacement of the beam at distance x
$\dot{v}_x$	Constant rate of beam opening at distance x
$\dot{v}_0$	Half of the test rate
x_0	Length of the straight portion of the tapered beam (i.e. 51.43mm)
Z	Thickness of the heat-affected zone
δ	Load-point displacement
δ_c	Constant opening displacement
$\dot{\varepsilon}_x$	Strain rate in the adhesive
ν_s	Poisson's ratio of the substrate
ν_a	Poisson's ratio of the adhesive
ω	Natural frequency of the beam
ρ_s	Density of the substrate
ρ_a	Density of the adhesive
σ_{CZ}	Cohesive strength
σ_y	Yield stress

INTRODUCTION

Adhesive bonding of lightweight, high-performance materials is regarded as a key enabling technology for the development of vehicles with increased crashworthiness, better fuel economy and reduced exhaust emissions. However, as automotive structures can be exposed to impact events during service, it is necessary to gain a sound understanding of the performance of adhesive joints under different rates of loading. This is of particular importance since adhesives for automotive applications are based on structural, toughened epoxy polymers that exhibit rate-dependent deformations [1-5]. Characterising the behaviour of adhesive joints as a function of loading rate is therefore critical for assessing and predicting their performance and structural integrity over a wide range of conditions.

A number of authors have employed finite-element analysis (FEA), with a cohesive-

zone model (CZM), to model the fracture of adhesively-bonded joints [e.g. 6-14]. There are also a limited number of publications in the adhesive fracture area involving the use of a finite volume method (FVM) and a CZM [15-17], and analytical solutions with a CZM [14, 18]. The CZM has two key parameters, namely the area under the traction versus separation curve (i.e. the adhesive fracture energy) and the maximum traction (i.e. the cohesive strength). Rate-dependent CZMs have been used extensively to model the fracture of rate-dependent materials in general [e.g. 19-29].However, only a few authors have reported the use of rate-dependent CZMs to study the fracture of adhesive joints [15, 30-35]. For example, to capture the rate-dependency of failure in adhesive bonds of the double cantilever-beam test specimen, Xuet. al. [30, 31] introduced a rate-dependent CZM based on the viscoelastic standard linear-solid model. Also, Georgiou et al [15] assumed a linear variation of the key CZM parameter, i.e. the adhesive fracture energy, with crack velocity to predict the fracture of tapered-double cantilever-beam (TDCB) joints, while bi-linear and parabolic approximations of G_{Ic} as a function of crack velocity were employed in [35]. In both [15] and [35] the cohesive strength was assumed to be equal to the ultimate tensile strength of the adhesive, and its variation with rate was extracted from experimental stress-strain curves obtained at different rates. Sun et al [32-34] reported that the mode I properties of the adhesive were almost rate-independent, until the crack velocity increased such that a transition to a brittle fracture occurred. At this transient, the mode I fracture energy dropped almost by a factor of four (i.e. from about 4.2 to 1.05 kJ/m^2), whilst the corresponding cohesive strength varied from about 21 MPa to about 27 MPa. On the other hand, the mode II fracture energy, somewhat strangely, increased with rate (from about 8 kJ/m^{2}to 24 kJ/m^2) and the corresponding shear strength varied from about 21 MPa to about 50 MPa [see Table 1 in 34].

Unstable, stick-slip crack propagation in adhesive joints is characterised by periodic crack jump-arrest regions and corresponding saw-tooth shape load versus time (or displacement) relationship and has been widely reported [e.g. 15, 32-36]. In order to predict stick-slip behaviour using a FEA CZM approach, Sun et al [32, 33] assumed an initial region ahead of the crack tip with a CZM toughness much higher than that in the rest of the specimen (i.e. by a factor of about five). The choice of the length of this region and toughness was based on trial and error and it was hence rather arbitrary. In [15, 35], the variation of G_{Ic} with crack velocity was assumed to be either linear, bi-linear or parabolic until a good prediction of the stick-slip behaviour was achieved. In [36] stick-slip propagation was not explicitly modelled and the values of G_{Ic} deduced were based on an analytical energy approach [18], and the effect of loading rate on the value of G_{Ic} was discussed in terms of a adiabatic thermal-heating model (ATM) [36]. In [37, 38], a non-monotonic fracture energy versus crack velocity curves were postulated. In [37], second- and third-order polynomials were assumed, whilst in [38] the stick-slip behaviour was described in terms of viscoelastic losses and a fracture energy versus velocity curve was obtained by superposition of a brittle fracture curve with a viscoelastic losses curve (based on Maugis [39]). It should be noted that there was no experimental justification for the assumed G_{Ic} dependency on the crack velocity in either [37] or [38].

The present work investigates the rate-dependent behaviour of adhesive joints under mode I loading conditions. A series of fracture tests were conducted using TDCB specimens at various loading rates [36, 40]. A high-velocity video camera was used to monitor the fracture events, i.e. to record the crack-length history, while a piezo-electric load-cell positioned closely to a lower arm of the specimen recorded the variation in load as a function of time. The experiments were analysed analytically and numerically. The full

details of the analysis strategy employing analytical approaches for different types of fracture are presented in [36]. The numerical modelling of the TDCB experiments was performed using the FVM based package 'OpenFOAM' [41]. The CZM employed was a Dugdale-shaped traction-separation law, and was applied as a traction boundary condition along a prospective crack plane. This type of CZM has been previously found to fit well the experimentally measured load versus displacement data [15, 25]. The initial region of the traction-separation law is taken as rigid. Two parameters, the adhesive fracture energy G_{Ic}, and the maximum traction, i.e. the cohesive strength, σ_{CZ}, are then sufficient to define the traction versus separation law. For the form of G_{Ic} for the rate-dependent CZM, the value of G_{Ic} as a function of crack velocity was obtained by fitting an appropriate curve through the G_{Ic} versus crack velocity data reported in [36, 40].

THE MATERIALS AND THEIR CHARACTERISATION

Substrates

A high-yield strength aluminium-alloy (EN-AW2014A) was used to manufacture the TDCB substrates. This ensured that the substrates remained within the elastic region throughout the tests, and so enabled valid linear-elastic fracture-mechanics test conditions. The aluminium-alloy beams were degreased in a trichloroethylene bath and the bonding surfaces were grit-blasted with 180/220 μm mesh grit. The beams were then etched in a chromic-sulphuric acid bath at 68˚C [40]. The relevant mechanical properties for this alloy are given in Table 1, where E_s is the Young's modulus, σ_y the 0.2% proof yield stress, *UTS* the ultimate tensile strength, ρ_s the mass density and ν_s the Poisson ratio. For the range of test rates employed in the current work, the properties of the aluminium-alloy are assumed to be rate independent.

Adhesive

A structural-epoxy adhesive, 'Betamate XD4600' supplied by Dow Automotive Europe, was used for the current research. This is a rubber-toughened single-part epoxy used primarily in automotive components. The adhesive was cured at 180˚C for 30 minutes. The adhesive glass transition temperature, T_g, is 118°C, and the mass density, ρ_a, and Poisson's ratio, ν_a, are 1300 kg/m^3 and 0.4, respectively [40, 42].

Uniaxial-tensile tests were conducted to obtain the basic mechanical properties of the adhesive over a wide range of test rates [40, 42]. Standard dumb-bell specimens were manufactured from a bulk 4 mm thick adhesive plate according to [43]. Tests were conducted at room temperature and a constant crosshead rate ranging from 1.67 x10^{-7} m/s to 5 m/s, corresponding to strain rates from 2.27 x10^{-6} s^{-1} to 66.67 s^{-1}, respectively. At low crosshead rates up to 0.1 m/s, the strains were measured using an electronic extensometer, while at rates above 0.1 m/s two strain gauges were used, one on each side of the gauge length. The low velocity tests were conducted using a screw driven Instron machine and a servo-hydraulic Instron was used for the high-rate tests. The values of Young's modulus E_a and *UTS* of the adhesive as a function of strain-rate are summarized in Table 2, and in Figures 1(a) and 1(b). It can be seen that both the *UTS* and E_a increase almost linearly with the logarithmic strain-rate.

FRACTURE TESTS

Introduction

The mode I adhesive fracture energy, G_{Ic}, was measured using TDCB test specimens, with the adhesive layer having a thickness of 0.4 mm and all other dimensions as shown in Figure

2. A polytetrafluoroethylene (PTFE) starter precrack was placed in the adhesive layer at the loading end. The length of the precrack measured from the loading line was 100 mm [40]. The profile of the arms was machined such that the rate of change of compliance increases linearly with the crack length and hence the derivative of the compliance will remain constant with increasing crack length. The beams were contoured to the profile described by the following equation:

$$m = \left(\frac{3a^2}{h_s^3} + \frac{1}{h_s} \right), \tag{1}$$

where h_s is the height of the substrate beam at distance $a \geq 51.43$ mm from the load-line, and a is the crack length. In the present work the geometry constant $m = 2$ mm^{-1} was used. All tests were performed under controlled conditions of approximately 50% relative humidity and a temperature of 23 ± 1°C.

Slow-Rate Tests

Slow-rate (i.e. quasi-static) tests up to crosshead rates of 0.1 m/s were undertaken using a displacement-controlled tensile-test machine ('Instron Model 1185' UK). The crack length was determined visually using a travelling microscope with sufficient magnification to allow readings of ±0.5 mm to be taken. Precracked TDCB joints were tested until a crack growth of approximately 105 mm was obtained. The load and the loading-point displacement were recorded at almost every millimetre of crack growth. At least four replicate tests for each joint system were tested. The tests were carried out according to the ISO 25215 procedure [44].

High-Rate Tests

An 'Instron VHS' high-rate servo-hydraulic machine was used to test the joints at crosshead rates between 0.1 m/s and 13.5 m/s. The machine was fitted with a lost motion device (LMD), which allowed adequate ram acceleration prior to specimen loading. The LMD and other fixtures were manufactured from titanium and aluminium alloy, in order to reduce inertial effects during testing. Additionally, a damping unit consisting of a set of hard rubber washers and a cup-and-cone connector was used to reduce contact effects between the ram and the lost motion device, see Figure 3.

The opening displacement at the loading points and the crack length were measured from the video sequence obtained from two high-speed video cameras. The 'Phantom 4' camera [45] was used to record slow to medium speed tests and the more advanced 'Phantom 7.1' camera was used for the higher rate tests where faster framing rates and higher picture resolution were imperative for accurate results. The framing rate used varied between 4,000 and 26,000 frames per second, giving not less than 10 frames for each test. The time-scale used for the determination of test rate and average crack velocities was based on the time-frame intervals. A high natural frequency and short rise-time piezo-electric load cell was attached immediately below the lower specimen arm for load measurements. Its output signal was amplified and fed into data acquisition equipment with a synchronised video feed. The recorded load versus time and crack length versus time traces are presented for a number of test rates below.

Types of Crack Growth

Different types of crack growth behaviour were observed over the range of test rates that were studied [36]. However, the crack propagated cohesively in the adhesive in all the tests. At relatively low loading rates up to about 0.1 m/s, the crack propagated in a stable, steady-state manner. This type of crack behaviour is denoted as 'Type 1'. At somewhat higher rates, between about 0.1 m/s and 2.5 m/s, the crack propagated in an unstable, stick-slip fashion, termed 'Type 2'. The stick-slip, unstable, crack growth behaviour consists of alternating periods of sudden high-velocity crack jumps followed by crack arrests which are visible as stress whitening marks on the fracture surfaces [46]. The stick-slip crack growth is usually accompanied by characteristic 'saw-tooth' shape load traces. Following the sudden jump, which is much faster than the loading rate, the crack 'runs out' of the available crack driving force and it arrests. The fast crack jumps are associated with smooth fracture surface regions. Subsequent loading, which is characterised by the whitening marks, provides the crack with the energy for the subsequent jump. The whole process then repeats itself in a periodic fashion. At even higher rates of test from about 2.5 m/s to 6.0 m/s the unstable crack propagation behaviour was still observed but it was considered that dynamic effects were now important, and hence it was termed 'Type 3' crack behaviour. At test rates above about 6.0 m/s, crack propagation was relatively rapid but stable once more, despite the mounting dynamic effects that produced progressively more severe oscillations in the load versus time traces. This was termed 'Type 4' crack growth. Table 3 summarises the four fracture types and indicates the approximate range of testing rates, and resulting average crack velocities, for each type. (It should be noted that the test rates associated with the various types of crack propagation are approximate to within about ±5%.)

Analytical Approach to Determining the Values of G_{Ic}

The different types of fracture described above require different analysis approaches in order to determine the values of the adhesive fracture energy from the measured values such as load, displacement, crack history etc. However, the standards developed for the TDCB test are only applicable at slow rates of loading and, ideally, for stable crack growth [47], i.e. quasi-static fracture such as 'Type 1'. For the 'Type 1' fracture, the stable propagation load and corresponding crack length values were employed to calculate G_{Ic} (see Table 4 [36]). In the present work, the same analysis is applied for the 'Type 2' fracture but, due to the stick-slip nature of the crack growth, initiation values of the load and corresponding crack length are used in the analysis. Hence, this approach gives initiation fracture energy values. (An alternative is to use the load and crack length values at arrest, which would result in lower-bound fracture energy results, but whose physical meaning is debatable [36].) The average crack velocity was obtained by finding a slope of a line fitted through (i) the propagation crack length values versus time, and (ii) the initiation crack length values versus time data for the 'Type 1' and 'Type 2' fractures, respectively.

There are no agreed standards for the analysis of tests at high rates which are associated with strong dynamic effects, which involves the propagation of stress-waves and considerable kinetic energy expenditure; and such effects are considered important if they exceed greater than about 5% of the quasi-static fracture energy G_{Ic} [36, 48, 49]. In order to avoid the dynamic effects present in the measured load traces a load-independent analysis has been employed to analyse the 'Type 3' and 'Type 4' fractures (see Table 4). Here, the load-line displacement and crack length values were used instead. The required values of load-line displacement, crack length and time were obtained from the high-speed videos. The average test rate was obtained by finding a gradient of the best linear fit to the load-line displacement history data. The average crack velocity was obtained by finding a slope of a

line fitted through (i) the initiation crack length values versus time data, and (ii) the propagation crack length values versus time data for the 'Type 3' and 'Type 4' fractures, respectively. The relationship between the average test rate and the average crack velocity is shown in Figure 4. Table 3 also indicates the approximate range of average crack velocities for the different fracture types. The different analysis strategies for the different types of fracture are explained in detail in [36]. It should also be noted, that the original dynamic analysis for the TDCB geometry proposed in [48] has been modified to account for the straight portion of the TDCB profile, x_0, and to incorporate the crack length correction, a^*, as proposed in [14].

By applying the analysis strategies described above to the experiments using the TDCB specimens, the fracture energy values are obtained as a function of the test rate (Figure 5(a)) and as a function of crack velocity (Figure 5(b)). Some scatter in the results is apparent from Figure 5 and it increases with the test rate (and the crack velocity). This is expected due to the increased dynamic effects and associated uncertainties in measurement of the experimental data such as load, displacement and the crack history at higher loading rates, and corresponding high crack velocities.

FINITE VOLUME MODELLING: CALIBRATION OF PARAMETERS

Introduction

The FVM was used for the numerical simulation of the experiments. This method was shown to be particularly suitable for modelling dynamic fractures [15-17, 27, 50-54] and problems involving fluid-solid-fracture interactions [55-58]. A fully implicit time-differencing scheme is employed in the analysis, which guaranties unconditional stability. The model was implemented using the 'OpenFOAM' package, which is a C++ library for continuum mechanics [41].

The adhesive was modelled as an elastic-plastic material using classical incremental J2 flow theory with von Mises plasticity, while the aluminium-alloy substrate was assumed to be linear-elastic throughout the analysis. Plane-stress conditions are assumed to dominate through the specimen thickness, and hence 2D calculations are performed. Due to two symmetries, only one quarter of the TDCB specimen is modelled. The numerical mesh typically used in the simulations is shown in Figure 6. The mesh consists of 14380 cells with uniform rectangular cells in the adhesive region of 0.5x0.04 mm. It should be noted here that a special care was taken in achieving converged, i.e. mesh and time step independent, results. The following time steps ensured time independent results: test rate - time step = 3.33×10^{-6} m/s - 50 s, 0.72 m/s – 0.2 ms, 1 m/s – 0.2 ms, 2.5 m/s – 50 μs, 5 m/s - 25 μs, 8.3 m/s - 7 μs, 9.6 m/s - 7 μs, 13.2 m/s - 5 μs. The mesh sensitivity study was demonstrated using the 3.33×10^{-6} m/s test (Figure 7(a)) and the time sensitivity study using the 9.6 m/s test (Figure 7(b)). From Figure 7(a) it may be seen that increasing the mesh density from 9512 cells to 87328 cells, with the aspect ratio of the adhesive cells size ranging from 12.5:1 (0.625x0.05 mm) to 2.5:1 (0.1x0.04 mm), respectively, had only marginal effects on the predicted load trace at a low loading rate of 3.33×10^{-6} m/s. During the crack propagation stage, the number of activated cohesive cell faces in front of the crack tip, i.e. the cohesive faces in the separation stage, ranged from around 10 for the coarsest mesh to around 50 for the finest mesh. This ensured accurate representation of the fracture process for all the meshes. The same conclusion applies for the higher loading rates. The effects of the time-step size were found insignificant at quasi-static loading rates below 1 m/s. However, at a relatively high loading rate of 9.6 m/s when the time step was reduced from 10 μs to 2μs the

average load remained largely unaffected while the oscillations in the predicted load traces became more pronounced at smaller time steps (Figure 7(b)).

Only mode I fractures were modelled by applying the CZM traction versus separation law along a prospective crack path in the mid-plane of the adhesive. Before the normal tractions on the prospective crack-path cell face reach the cohesive strength, the cohesive surface behaves in the same manner as the surrounding bulk material, and it is modelled as a symmetry plane using mixed boundary conditions. After the stress level reaches the cohesive strength, σ_{CZ}, representing the initiation of damage, the material behaves according to the prescribed Dugdale CZM traction-separation law. The entire cell-face is assumed to be fractured when twice the normal cell face separation reaches its critical value and the tractions are dropped to zero.

Material properties

The adhesive mechanical properties were found to be rate dependent (see Table 2 and Figure 1) whilst no rate sensitivity of the substrate material was observed for the range of test rates employed in this work (see Table 1). In order to find the appropriate material properties of the adhesive for the simulation of TDCB experiments at different rates, it is first necessary to estimate the strain rates near the crack tip region in the TDCB specimen. Then, the appropriate properties for the numerical simulations can be found by matching the TDCB strain rates with those from uniaxial-tensile tests. Initially, the strain rate at the crack tip in the loading direction as a function of test rate was approximated using an analytical beam on an elastic-foundation approach [59]. One half of the TDCB sample was approximated using an elastic beam with a uniform rectangular cross section of b x h_{beam} = 10 x 16 mm corresponding to the initial straight arm of the TDCB sample (Figure 2), i.e. the TDCB geometry is approximated as DCB geometry. The length of the beam is set to L = 300 mm, i.e. it is taken equal to the length of the TDCB sample measured from the load-line. Linear springs of stiffness k are applied over the un-cracked length of the beam for $x \geq a_0 = 105$ mm, where x is a distance along the beam measured from the load-line. The strain rate in the adhesive at a distance x can be approximated as:

$$\dot{\varepsilon}_x = \frac{\dot{v}_x}{h/2} = \frac{2v_x\dot{v}_0}{hv_0}, \tag{2}$$

where: $\dot{v}_x = v_x/t$ constant rate of beam opening at distance x, t is time, h adhesive thickness, $\dot{v}_0 = V/2$ half of the test rate (only half of the sample was modelled), v_x the displacement of the beam in loading direction at distance x given as:

$$v_x = e^{\omega x}\left(C_1 \sin \omega x + C_2 \cos \omega x\right) + e^{-\omega x}\left(C_3 \sin \omega x + C_4 \cos \omega x\right), \tag{3}$$

where:

$$\omega = \sqrt[4]{\frac{k}{4E_s I_s}}, \quad k = \frac{2E_a b}{h}, \quad I_s = \frac{bh_{beam}^3}{12} = \frac{10 \cdot 16^3}{12} \text{ mm}^4$$

and C_i (i= 1 - 4) are the constants of integration obtained from boundary conditions:

$$v_0 = \dot{v}_0 t, \quad v_0'' = 0, \quad v_L'' = v_L''' = 0 \quad (v' = dv/dx).$$

By setting $x = a_0$ in the above, where $a_0 = 105\text{mm}$, one can get the strain-rate at the crack tip as a function of the test rate. The analytical estimates of the strain-rates are used to obtain the 'first estimate' of the mechanical properties for the numerical estimate of the strain-rates as a function of the test rate. Here, the TDCB specimen is modelled in an iterative manner without the CZM (the crack plane is assumed as a symmetry plane) at various applied test rates from 0.1 to 13.5 m/s. During the calculation, the accurate strain-rates at the crack tip cell are calculated and the materials properties adjusted according to the uniaxial-tensile test rates until a converged solution is obtained. Table 5 summarises the strain-rates as a function of the test rate from the analytical and numerical calculation, and the general agreement between these two modelling methods was found to be good. The corresponding adhesive mechanical properties are obtained from uniaxial-tensile tests (Table 2 and Figure 1) by matching the strain-rates from the numerical TDCB calculations. These properties are used in the FVM/CZM simulations of the TDCB fracture tests conducted at the various test rates.

It should be noted that the numerical modelling requires mechanical properties at strain rates outside of the range of the measured values. These data were found by means of linear interpolation (for rates between the measured points) and linear extrapolation (for rates below and above the measured points) of the experimentally measured data, and are plotted alongside the directly measured data in Figure 1 (but noted as estimated data). Also shown in Figure 1 are the data points used in the FVM simulations, as given in Table 5.

The CZM

In order to simulate the TDCB fracture tests, one also needs to prescribe the CZM parameters as a function of rate. The cohesive strength, σ_{CZ}, was assumed to be equal to the value of the *UTS* of the adhesive at the corresponding strain-rate (Table 5). This choice is based on the authors' previously reported work [15, 35]. The reasoning behind this choice is that the stress under which the material will fail under uniaxial conditions is equal to the *UTS*. Under uniaxial conditions, the constraint factor $H = \sigma_H / \sigma_{eff} = 1/3$, where σ_H is the hydrostatic stress and σ_{eff} is the effective stress. In general $H \geq 1/3$ and hence the minimum separation stress is equal to *UTS*. However, the crack tip region is normally expected to be under a highly triaxial state of stress and for the TDCB geometry *H* was reported to vary from 1.5 at 2 mm bond-gap thickness to 2.3 at 0.25 mm bond-gap thickness [7, 60], where a cohesive strength of up to 3x*UTS* might be expected. Although G_{Ic} was found to vary considerably with *H*, the cohesive strength was found to be relatively insensitive to the variation in *H* and only reached 1.5x*UTS* at *H* = 2.3 [60]. In the current work, the constraint factor was found to be around 1.0 for an adhesive layer thickness of 0.4 mm, which is below the value reported in [60]. This is due to different adhesives employed in the two studies which exhibited different behaviour and the plane-strain assumption used in [60]. In the current work, pronounced plasticity was observed throughout the adhesive layer in the crack tip region, which was not the case with the results reported in [60]. The effects of the variation of σ_{CZ} from *UTS*=61.9 MPa to 3x*UTS* have been examined and the results are shown in Figure 8(a) for a test rate of 3.33×10^{-6} m/s with a corresponding value of G_{Ic}=3.7 kJ/m^2. It can be seen that the experimentally measured load and crack length versus displacement curves are best predicted with the value of σ_{CZ} taken to be similar in value to the *UTS*, especially for the load versus displacement data. This observation is in agreement with previously reported results in [7, 15, 35].

NUMERICAL PREDICTIONS OF TDCB FRACTURE TESTS

A Rate-Independent CZM

Initially, numerical simulations were conducted with a constant value of the adhesive fracture energy for the given rate of test, i.e. the value of G_{Ic} is taken from Figure 5(b) for a given (average) crack velocity from the linear data-fit line. When attempting to predict the stable types of crack growth, i.e. fracture 'Type 1' and 'Type 4', the rate-independent, constant G_{Ic} approach resulted in reasonable numerical predictions of the experimentally recorded load and crack length versus load-line displacement curves. For example, Figure 8(b) shows the comparison between the numerical and experimental results for a test rate of 3.33×10^{-6} m/s, with a corresponding value of G_{Ic}= 3.7 kJ/m^2.

However, numerical simulations with G_{Ic} held constant to a particular value corresponding to a selected test-rate/crack-velocity were not successful in predicting the unstable 'Type 2' and 'Type 3' fracture behaviour, particularly the 'Type 2' behaviour which exhibited strong stick-slip behaviour. Here, the predicted load and crack length traces were smooth in nature and only agreed with the experimental data in an average sense and, most importantly, the stick-slip behaviour was not reproduced. For example, this is clearly demonstrated in Figure 9 for a test conducted at 0.72 m/s, where 'Type 2' fracture was observed. Now, from Figure 5(a) the value of G_{Ic} was firstly kept constant to a value of 3.7 kJ/m^2 and the stick-slip load versus displacement behaviour is not predicted at all, and the numerical predictions somewhat overestimate the load recorded experimentally. This is to be expected as the G_{Ic} value used in the numerical simulations for 'Types 2 and 3' behaviour is based on the analytical-calculated values given in Figure 5, which are obtained from the load values at initiation only (Table 4) and for an 'averaged' crack velocity over the many discontinuous stick-slip fracture events. Secondly, in order to further demonstrate this point, two additional simulations were conducted: (i) with G_{Ic}=2.6 kJ/m^2, this value being based on the average load, and (ii) with G_{Ic}=1.7 kJ/m^2, this value being based on the load at arrest; The load values used in the 'Type 2' equation in Table 4 are taken from the experimental saw-tooth shaped load versus displacement trace while the corresponding crack length is taken from the experimental crack length versus displacement trace, i.e. the average crack length between the initiation and arrest point is taken for the average load calculation, and the crack length at arrest is taken for the load at arrest calculation. As may be seen from Figure 9(a), the corresponding numerical simulations result in mid- and lower-bound predictions of the load versus displacement traces, when compared to the experimental traces. Finally, the predictions shown in Figure 9 also reveal the strong effect that the inputted value of the adhesive fracture energy, G_{Ic}, for the CZM has on the numerical predictions.

A Rate-Dependent CZM

In the above it was clearly demonstrated that a CZM with a G_{Ic} value held constant, corresponding to a particular test rate and hence fixed to a corresponding average crack velocity, could not predict the stick-slip fracture behaviour. In order to overcome this problem, it was decided to use a CZM approach with a rate-dependent G_{Ic} term. A number of relationships were fitted to the G_{Ic} versus crack velocity data presented originally in Figure 5(b) and a selected number of the attempts are shown in Figure 10. It should be noted that the experimental data points given in Figure 10 for the unstable, stick-slip types of fracture are based on values of G_{Ic} calculated from values of the load for the onset of crack growth, i.e. crack initiation, and the crack velocity employed is the average crack velocity, as discussed above. This may result in somewhat overestimated G_{Ic} values for the stick-slip fracture types.

In Figure 10, 'Profile D' corresponds to the linear fit through the data points, as shown

in Figure 5. 'Profiles A to C' assume an initial rapid decrease of G_{Ic} with crack velocity at low crack velocities from 0 to 20 m/s for 'Profile A' and 'Profile C' and from 0 to 60 m/s for 'Profile B', followed by a less steep linear decrease to a value of 2.5 kJ/m^2 at 400 m/s. The rate of decrease of G_{Ic} with crack velocity is the highest for 'Profile A' and lowest for 'Profile B', with 'Profile C' lying in between these two. These three profiles were taken below the linear fit ('Profile D') to address possible overestimation of G_{Ic} in the stick-slip fracture regimes ('Types 2 and 3') but are well within experimental G_{Ic} data at low ('Type 1') and high crack velocity regimes ('Type 4') where such overestimation is not expected. The expansion of the initial region of all the profiles is also shown in Figure 10(b) for clarity. In addition to these four profiles fitted to experimental data, two additional profiles named 'ATM' are also analysed. These profiles are obtained from an adiabatic thermal-heating model (ATM) with the values of the thickness, *Z*, of the heat-affected zone being 25 or 75 μm [36]. The details of the model are presented in [36, 40], where a transition from isothermal to adiabatic conditions at the cack tip, as the test rate is increased, is proposed and modelled. The model is based on the proposal that the variation of G_{Ic} with rate (either test rate and/or crack velocity) is related to the localisation of heat in the region close to the crack tip (i.e. the heat affected zone). It is assumed that the fracture energy, G_{Ic}, is converted into heat and that fracture occurs at a constant opening displacement δ_c, where $G_{Ic} = \sigma_y \delta_c$; and σ_y is the yield stress which is assumed to vary linearly with temperature. At relatively low test rates the heat has sufficient time to be conducted away from the crack tip region, resulting in isothermal conditions with no significant temperature rise around the crack tip. At relatively high test rates, the transition from isothermal to adiabatic conditions occurs around the crack tip due to insufficient time for heat to be conducted away through the adhesive, resulting in a significant local temperature rise. The details of this approach, the model and the relationships shown for the 'ATM' profiles shown in Figure 10 are given in [36].

In what follows, the various G_{Ic} versus $\dot{a}$ profiles, as shown in Figure 10, were implemented into the FVM/CZM procedure described above and employed to simulate all the fracture types, i.e. the stable 'Type 1' and 'Type 4' fracture behaviour and the unstable 'Type 2' and 'Type 3' fracture behaviour. At the beginning of each time step, the crack velocity estimated from the previous time step is used to obtain the new value of G_{Ic}, from the prescribed G_{Ic} versus $\dot{a}$ relationship. At the initiation of fracture, the crack velocity is zero, and the calculation starts with G_{Ic} at zero crack velocity. The process is repeated, i.e. marched in time, until the entire TDCB joint was fractured.

The following sections present the results from the FVM/CZM simulations of the TDCB tests conducted at test rates of 3.33 x 10^{-6} m/s (where 'Type 1' fracture behaviour was recorded), 0.72 m/s ('Type 2'), 2.5 m/s ('Type 3') and 9.6 m/s and 13.5 m/s (both 'Type 4'). Further, as explained in the previous section, (i) the value of σ_{CZ} was varied according to the test rate employed, see Table 5, whilst (ii) 'Profiles A, B, C, D and ATM *Z* = 25 and 75 μm', see Figure 10, were employed, in turn, as the appropriate form for the G_{Ic} versus crack velocity relationship to use for the rate-dependent CZM in the FVM numerical simulations.

Figures 11, 12, 13, 14 and 15 show the results from these simulations using these rate-dependent relationships at test rates of 3.33 x10^{-6} m/s, 0.72 m/s, 2.5 m/s, 9.6 m/s and 13.5 m/s, respectively, with the load versus displacement traces given in (a) and the crack length versus displacement traces in (b). The simulations, using the different profiles, are compared to the experimental results in each case. The main observations regarding the

numerical predictions of the load and crack length versus displacement traces for the TDCB joints are summarised below for each type of fracture behaviour.

'Type 1' (Slow-rate, Stable)
At a test rate of 3.33 x10^{-6} m/s stable crack, 'Type 1' fracture behaviour, was observed, see Figure 11, and both the load and the crack-length traces are predicted very well. Indeed, the differences in the predictions from the different profiles assumed in Figure 10 for the G_{Ic} versus crack velocity relationship are almost negligible and hence cannot be readily distinguished in Figure 11. This is due to the fact that for all the profiles (i) the variation in the predicted crack velocity, and hence G_{Ic}, was very small at low loading rates, and (ii) all the profiles possess a very similar value of G_{Ic} at low crack velocities, i.e. G_{Ic}=3.6 kJ/m^2 for 'Profiles A, B, C and ATM Z = 25μm and Z =75 μm' and G_{Ic}=3.73 kJ/m^2 for 'Profile D' for a crack velocity approaching zero.

In order to explain the differences in numerical predictions when different profiles are employed, Figure 16 shows for each type of fracture the range of variation of the crack velocity as predicted in the numerical simulations when using the representative 'Profiles A, ATM Z = 75 μm and D'. Figure 16 indicates that for the 'Type 1' fracture, the predicted crack velocity is constant and equal to 7.1 x 10^{-5} m/s regardless of the G_{Ic} versus crack velocity profile employed. The experimentally recorded crack velocity is also found to be virtually constant throughout the stable propagation of the crack (see Figure 11(b)) and has an average value of 6.9 x 10^{-5} m/s. The agreement between the modelling studies and the experimental results is therefore also excellent in this respect.

'Type 2' (Slow-rate, Unstable)
At a test rate of 0.72 m/s slow-rate unstable stick-slip fracture was seen, i.e. 'Type 2' behaviour, see Figure 12. It is clear that 'Profile D' (i.e. a linear fit) does not predict these stick-slip fractures at all well. However, profiles with a relatively steep initial decrease in G_{Ic} with $\dot{a}$ (such as 'Profiles A, ATM Z = 25 μm and ATM Z = 75 μm') gave more pronounced stick-slip behaviour than the profiles with less steep initial decreases (such as 'Profiles B, C and D'). Indeed, 'Profiles A and ATM Z= 75 μm' gave reasonable predictions of the stick-slip fracture behaviour, while 'Profile ATM Z = 25 μm', which is a lower-bound fit to the G_{Ic} versus crack velocity data (see Figure 10), does not capture the dynamics, i.e. the number of oscillations in either the load or crack length traces. For the 'Profiles A and ATM Z = 75 μm', the number of main oscillations in the experimentally recorded saw-tooth shape load versus displacement curve is predicted relatively accurately but the amplitude of such oscillations predicted numerically is somewhat lower than that observed experimentally. The prediction of the crack-length history is much better than that of the load history, with 'Profiles A and ATM Z = 75 μm' giving the best results. It is believed that the inability of the numerical simulation to predict exactly the experimental load trace is due to dynamic effects of the machine-specimen system superimposed on the load trace. Indeed, it should be noted that the experimental load was recorded by the load cell placed a few centimetres below the lower arm of the TDCB specimen, and hence it captures the dynamics of the entire loading system and the specimen. In contrast, the numerical simulations predict the load directly from the specimen and so capture the dynamics of the specimen only. These factors lead to the apparently poor agreement between the numerical simulations and the experimental results, in terms of the exact number and extent of the minor oscillations experimentally recorded for the load versus displacement trace. These effects of the system dynamics are expected to increase, of course, with increasing test rate. Ideally, one should model a part or the entire loading system including the specimen to capture the dynamics of

the system and hence predict the load traces more accurately. This was outside the scope of the current work. However, the ability of the model to predict accurately the load histories at low test rates and locally measured crack histories for all the test rates investigated demonstrates the accuracy and predictive capability of the model for all rates.

Now, from Figure 16 it can be seen that the predicted crack velocity, and the corresponding value of G_{Ic}, vary considerably for 'Type 2' when 'Profile A' was used, i.e. the predicted crack velocity varies from 0 to 40 m/s with a corresponding G_{Ic} variation from around 3.6 to 2.97 kJ/m^2. Similarly, the simulation with 'Profile ATM Z =75 μm' resulted in a variation in crack velocity from 0 to 40 m/s, and a corresponding decrease in G_{Ic} from 3.6 to 2.95 kJ/m^2.This relatively large variation in G_{Ic} causes large corresponding variations in the predicted load (see also see Figure 9), and hence leads to the saw-tooth shape profile which represents the unstable, stick-slip fracture behaviour. When 'Profile D' was used, a very small variation of crack speed is predicted (i.e. 14.5 to 17 m/s) and the corresponding variation in G_{Ic} is small (i.e. 3.69 to 3.68 kJ/m^2), which results in only a small variation in the predicted load. Therefore, Figure 16 clearly demonstrates that for the stick-slip fracture 'Type 2', the variation in the crack velocity is associated with a large variation in G_{Ic} at low crack velocities between 0 and around 40 m/s when 'Profiles A and ATM Z =75 μm' are used. Hence, the 'Type 2' fracture behaviour could only be predicted accurately when 'Profiles A and ATM Z =75 μm' were used to describe the rate-dependence of the G_{Ic} value used in the CZM.

'Type 3' (Fast-rate, Unstable)

At a test rate of 2.5 m/s, high-rate unstable fracture was seen, i.e. 'Type 3' behaviour, see Figure 13.The load versus displacement curve for this test rate is of a highly oscillatory nature, which in the first instance may appear as the stick-slip characteristic saw-tooth shape, with a relatively large number of oscillations (see Figure 13(a)). However, the corresponding crack length versus displacement data does not correlate well with the load trace as it only shows two characteristic plateau regions of low crack velocity (see Figure 13(b)). The main reason for this mismatch in the load and crack length traces is believed to be due to the considerable dynamic effects superimposed on the actual load versus displacement trace. Apart from the 'Profile ATM Z = 25 μm', the predictions from all other profiles are in reasonably good agreement with each other and resemble the experimental data well, particularly for the crack length trace; with 'Profile A' giving somewhat the best predictions of both the load and crack length traces. Again, the load versus displacement trace is predicted in an average sense only, due to the machine dynamic effects present in the experimentally recorded load, and which are not accounted for in the numerical simulations.

It can be seen in Figure 16 that for the 'Type 3' fracture, the crack velocity varies from 20 to 80 m/s when using 'Profiles A and ATM Z =75 μm' and from 30 to 70 m/s when using 'Profile D'. The corresponding variation in G_{Ic} is from 3.0 to 2.9 kJ/m^2, 3.1 to 2.8 kJ/m^2 and from 3.6 to 3.5 kJ/m^2 for the 'Profiles A, ATM Z =75 μm and D', respectively. However, the variations in G_{Ic} are not as large as for the 'Type 2' fracture with the 'Profiles A and ATM Z =75 μm'. The corresponding variation in the load, and hence the stick-slip behaviour, is therefore not as pronounced as for the 'Type 2'. The load predictions using 'Profile D' are somewhat higher than when using 'Profiles A and ATM Z =75 μm'. This arises because of the higher G_{Ic} associated with 'Profile D', but a similar variation in G_{Ic} for the other two profiles ensures similar behaviour of the predicted load traces (see Figure 13(a)).

'Type 4' (Fast-rate, Stable)
At test rates of 9.6 m/s and 13.5 m/s, then stable crack growth was again observed, i.e. 'Type 4' crack behaviour in both cases (see Figures 14 and 15). As for the 'Type 1' and 'Type3' fracture behaviour, all the profiles predict the experimental load and crack length traces in a similar fashion.

The variation in the crack speed and corresponding G_{Ic} are shown in Figure 16 for the predictions with the 'Profiles A, ATM Z =75 μm and D'. The crack velocity varies from 200 to 330 m/s when using 'Profile A' and from 230 to 330 m/s when using 'Profile D'. The corresponding variation in G_{Ic} is from 2.8 to 2.6 kJ/m^2, and from 3.0 to 2.7 kJ/m^2 for the 'Profiles A and D', respectively. The simulation with 'Profile ATM Z =75 μm' predicted almost a constant crack velocity of 270 m/s with G_{Ic}= 2.8 kJ/m^2 (see Figure 16). As for the 'Type 3' fracture, the variations in G_{Ic} between the three profiles are similar and hence the similarity in predicted load and crack length traces. Whilst the predicted crack length versus displacement traces closely resemble the experimentally recorded traces, the agreement between the predictions and measurements of the load versus displacement curves gets progressively worse with increasing test rate. This is expected as uncertainties, particularly in the load history measurements, increase with increasing test rate due to more pronounced dynamic effects of the entire machine-specimen system which obscures the 'true' load trace.

Further, Figure 17 demonstrates that a rate-independent (i.e. constant) G_{Ic} approach also predicts quite well the high-rate stable fracture behaviour (i.e. 'Type 4'). Here the results are for a test conducted at 9.6 m/s and the constant value of G_{Ic} is taken to be 3.01 kJ/m^2. This value is taken from the linear-fit (i.e. 'Profile D') at the average crack velocity of 250 m/s.

Concluding Comment
Finally, it should be noted that in all cases, the numerical simulations show a sudden decrease in the load, and a corresponding 'jump' in the crack length, as the crack approaches the last quarter of the length of the specimen. It is well known that the crack does indeed 'jump' in the last quarter of the TDCB joint specimen, and this is particularly pronounced at relatively low test rates. Hence, experimental measurements are normally ceased before the crack approaches this region. However, in the numerical simulations the crack is allowed to propagate along the entire specimen length.

CONCLUSIONS

The present paper has presented a combined experimental, analytical and numerical-modelling study of the mode I fracture behaviour of tapered double-cantilever beam (TDCB) bonded joints subjected to a range of test rates between 3.33 x 10^{-6} m/s and 13.5 m/s. The TDCB joints were manufactured from aluminium-alloy substrates bonded together using a single-part, rubber-toughened, epoxy adhesive. All the tests failed via the crack propagating cohesively along the centre of the adhesive layer. Different types of fracture behaviour where observed depending on the test rate: 'Type 1' slow-rate, stable crack growth at test rates below 0.1 m/s; 'Type 2' slow-rate, unstable stick-slip fracture at test rates between 0.1 m/s and 2.5 m/s; 'Type 3' high-rate, unstable stick-slip fracture at test rates between 2.5 m/s and 6 m/s; and 'Type 4' high-rate, stable crack growth at test rates above 6 m/s.

The experiments were analysed analytically, via linear-elastic fracture mechanics methods [36] and numerically. In the analytical study, different approaches were required for the different fracture types. 'Type 1' and 'Type 2' fracture behaviour were analysed using a quasi-static approach: with the measured crack propagation loads being used for 'Type 1' and the measured load at crack initiation being used for 'Type 2'. Dynamically-corrected analyses, based on the crack length instead of the load, were employed to determine G_{Ic} values for 'Type 3' and 'Type 4' fracture behaviour. Again, crack initiation data were used for the unstable 'Type 3' fractures, while crack propagation data were employed for the stable 'Type 4' fractures. Numerical simulations were conducted using the finite-volume method (FVM) based package 'OpenFOAM', with an embedded cohesive-zone model (CZM), based upon a Dugdale shape. The CZM employed either (i) a rate-independent, or (ii) a rate-dependent value of G_{Ic}. The uniaxial-tensile properties and the adhesive fracture energy, G_{Ic}, for the adhesive were measured and calibrated at the appropriate strain-rates. In the CZM, the maximum traction (i.e. the cohesive strength, σ_{CZ}) was assumed to be equal to the value of the ultimate tensile strength (UTS) of the adhesive at the strain-rate corresponding to the test rate of interest. When a rate-independent value for G_{Ic} was used in the CZM, then a constant value of G_{Ic} was selected which corresponded to the measured average crack velocity for the crack propagating through the adhesive layer of the TDCB joint. When a rate-dependent value of G_{Ic} was employed in the CZM, then various forms for the G_{Ic} versus average crack velocity, $\dot{a}$, 'profiles' were assumed in the numerical simulations. These were obtained from (i) assuming the best-fit experimental, (ii) trial and error assumptions, and (iii) an adiabatic thermal-heating model (ATM), which has been previously proposed [36].

Two-dimensional plane-stress, elastic-plastic, fully-implicit transient analyses were performed and numerical predictions of the load versus displacement and crack length versus displacement traces were compared against the experimentally-measured traces. It was found that for stable fracture behaviour, i.e. 'Type 1' and 'Type 4', the load and crack-length traces were predicted very accurately using all the 'profiles' which were selected to describe the relationship between G_{Ic} and the average crack velocity, $\dot{a}$. Indeed, it was also found that a rate-independent (i.e. constant) value of G_{Ic} for the CZM gave good predictions of the experimentally-measured load and crack-length traces when stable fracture behaviour was observed. i.e. 'Type 1' and 'Type 4'. However, for the unstable, stick-slip fracture behaviour, i.e. 'Type 2' and 'Type 3', then the experimentally-measured load and crack-length traces were only successfully predicted using 'Profile A' and the profile based on the adiabatic thermal-heating model with the thickness, Z, of the heat-affected zone being 75 μm (i.e. 'Profile ATM Z = 75 μm'). The main characteristics of both of these profiles are (i) a rapid drop in the value of G_{Ic} at low crack velocities between ≅0 and 60 m/s (i.e. from about 3.5 kJ/m^2 at ≅0 m/s to about 3.0 kJ/m^2 at 20 m/s), followed by (ii) a steady decrease in G_{Ic} to about 2.5 kJ/m^2 at about 400 m/s (see Figure 10). Nevertheless, the numerical simulation of the 'Type 3' fracture did suggest that the large number of minor oscillations observed in the load versus displacement trace are largely due to the system dynamic effects superimposed on the 'true' load versus displacement trace, which the current FVM/CZM procedure fails to capture.

ACKNOWLEDGMENTS

The authors would like to thank the Irish Research Council for Science Engineering and Technology (IRCSET) and Henkel Ireland Ltd. for their financial support and Dow Automotive Europe for material supply. We also wish to thank the Mexican Government

(funding for FSRS) and the Singapore Government under the A-Star Scheme (funding for WST).

REFERENCES

1. Kinloch, A. J., Shaw, S. J., Tod, D. A., Hunston, D. L., Deformation and fracture behaviour of a rubber-toughened epoxy: I. Microstructure and fracture studies, *Polymer* **24** (1983), 1341-1354.
2. Kinloch, A. J., Shaw, S. J., Hunston, D. L., Deformation and fracture behaviour of a rubber-toughened epoxy: II. Failure criteria, *Polymer* **24** (1983), 1355-1363.
3. Hunston, D. L., Bullman, G. W., Viscoelastic fracture behaviour for different rubber-modified epoxy adhesive formulations, *Int. J. Adhesives & Adhesion* **5** (1985), 69-74.
4. Huang, Y., Kinloch, A. J., The use of time-temperature super positioning in studying the fracture properties of rubber-toughened epoxy polymers, *J. Adhesion* **41** (1993), 5–22.
5. Raghavan, D., He, J., Hunston, D., Hoffmann, D., Strain rate dependence of fracture in a rubber-toughened epoxy system, *J. Adhesion* **78** (2002), 723-739.
6. Wei, Y., Hutchinson, J. W., Interface strength, work of adhesion and plasticity in the peel test, *Int. J. Fract.* **93** (1998), 315-333.
7. Hadavinia, H, Kawashita, L., Kinloch, A. J., Moore, D. R., Williams, J. G., A numerical analysis of the elastic-plastic peel test, *Eng. Fract. Mech.* **73** (2006), 2324-2335.
8. Blackman, B. R. K., Hadavinia, H., Kinloch, A. J., Williams, J. G., The use of cohesive zone model to study the fracture of fibre composites and adhesively-bonded joints, *Int. J. Fract.* **119** (2003), 25-46.
9. Yang, Q. D, Thouless, M. D., Ward, S. M., Numerical simulations of adhesively-bonded beams failing with extensive plastic deformation, *J. Mech. Phys. Solids* **47** (1999), 1337-1353.
10. Li, S., Thouless, M. D., Waas, A. M., Schroeder, J. A., Zavattieri, P. D., Use of mode-I cohesive-zone models to describe the fracture of adhesively-bonded polymer-matrix composite, *Compos. Sci. Technol.* **65** (2005), 281–293.
11. Ferracin, T., Landis, C. M., Delannay, F., Pardoen, T., On the determination of the cohesive zone properties of an adhesive layer from the analysis of the wedge-peel test, *Int. J. Solids Structure* **40** (2003), 2889-2904.
12. Pardoen, T., Ferracin, T., Landis, C. M., Delannay, F., Constraint effects in adhesive joint fracture, *J. Mech. Phys. Solids*. **53** (2005), 1951–1983.
13. Martiny, P., Lani, F., Kinloch, A. J., Pardoen, T., Numerical analysis of the energy contributions in peel tests: A steady-state multilevel finite element approach, *Int. J. Adhesives & Adhesion* **28** (2008), 222-236.
14. Blackman, B. R. K., Hadavinia, H., Kinloch, A. J., Paraschi, M., Williams, J. G., The calculation of adhesive fracture energies in mode I: revisiting the tapered double cantilever beam (TDCB) test, *Eng. Fract. Mech.* **70** (2003), 233-248.
15. Georgiou, I., Ivankovic, A., Kinloch, A. J., Tropsa, V., Rate dependent fracture behaviour of adhesively bonded joints, *Fracture of Polymers, Composites and Adhesives* II, Eds. B. R. K. Blackman, A. Pavan, J. G. Williams, ESIS Publication **32**, Elsevier Ltd., (2003), 317-328.
16. Cooper, V., Ivankovic, A., Karac, A., 'Study of bond thickness effects on the mode I fracture toughness of adhesively bonded joints'. Proceedings of the 31st Annual Meeting of the Adhesion Society, Texas, February 2008.

17. Cooper, V., Ivankovic, A., Karac, A., Murphy, N., 'The effect of constraint on the fracture toughness of adhesively bonded joints'. Proceedings of the 32st Annual Meeting of the Adhesion Society, Savannah, February 2009.
18. Georgiou, I., Hadavinia, H., Ivankovic, A., Kinloch, A. J., Tropsa, V., Williams, J. G., Cohesive zone models and the plastically-deforming peel test, *J. Adhesion* **79** (2003), 239-265.
19. Cox, B. N., Gao, H., Gross, D., Rittel, D., Modern topics and challenges in dynamic fracture, *J. Mech. Phys. Solids*. **53** (2005), 565–596.
20. Foulk, J. W., Allen, D. H., Predicting time-dependent interfacial behaviour with a viscoelastic cohesive zone model, Int. Conf. on Computational Engineering Sciences ICES 2K, LA, USA, 2000
21. Allen, D. H., Searcy, C. R., A micromechanical model for a viscoelastic cohesive zone, *Int. J. Fract.* **107** (2001), 159-176.
22. Zhang, X., Mai, Y-W., Jeffrey, R. G., A cohesive plastic and damage zone model for dynamic crack growth in rate-dependent materials, *Int. J. Solids Structure* **40** (2003), 5819-5837.
23. Bazant, Z. P., Li, Y-N., Cohesive crack with rate-dependent opening and viscoleasticity: I. Mathematical model and scaling, *Int. J. Fract.* **86** (1997), 247-265.
24. Li, Y-N.,Bazant, Z. P., Cohesive crack with rate-dependent opening and viscoleasticity: II. Numerical algorithm, behaviour and size effect, *Int. J. Fract.* **86** (1997), 267-288.
25. Kubair, D. V., Geubelle, P. H., Huang, Y. Y., Analysis of rate-dependent cohesive model for dynamic crack propagation, *Eng. Fract. Mech.* **70** (2003), 685-704.
26. Roe, K. L., Siegmund, T., An irreversible cohesive zone model for interface fatigue crack growth simulation, *Eng. Fract. Mech.* **70** (2003), 209-232.
27. Ivankovic, A., Pandya, K., Williams, J. G., Crack growth predictions in polyethylene using measured traction – separation curves, *Eng. Fract. Mech.* **71** (2004), 657-668.
28. Ting, S. K. M., Williams, J. G., Ivankovic, A., Characterisation of fracture behaviour of polyethylene using measured cohesive curves. I: Effects of constraint and rate, *Polymer Eng. Sci.* **46** (2006), 763-777.
29. Ting, S. K. M., Williams, J. G., Ivankovic, A., Characterisation of fracture behaviour of polyethylene using measured cohesive curves. II: Variation of cohesive parameters with rate and constraint, *Polymer Eng. Sci.* **46** (2006), 778-791.
30. Xu, C., Siegmund, T., Ramani, K., Rate-dependent crack growth in adhesives I. Modeling approach, *Int. J. Adhesion & Adhesives* **23** (2003) 9-13.
31. Xu, C., Siegmund, T., Ramani, K., Rate-dependent crack growth in adhesives II. Experiments and analysis, *Int. J. Adhesion & Adhesives* **23** (2003) 15-22.
32. Sun, C., Thouless, M. D., Waas, A. M., Schroeder, J. A., Zavattieri, P. D., Rate effects for mixed-mode fracture of plastically-deforming adhesively-bonded structures, *Int. J. Adhesion & Adhesives* **29** (2009) 434-443.
33. Sun, C., Thouless, M. D., Waas, A. M., Schroeder, J. A., Zavattieri, P. D., Ductile-brittle transitions in the fracture of plastically-deforming, adhesively-bonded structures: I experimental studies, *Int. J. Solids Struct.* **45** (2008), 3059–73.
34. Sun, C., Thouless, M. D., Waas, A. M., Schroeder, J. A., Zavattieri, P. D., Ductile–brittle transitions in the fracture of plastically-deforming, adhesively-bonded structures: II Numerical studies. *Int. J. Solids Struct.*, **45** (2008), 4725–38.
35. Blackman, B. R. K., Cooper, V., Ivankovic, A., Karac, A., Kinloch, A. J., Rodriguez Sanchez, S., Teo, W. S., Stick-slip crack propagation in adhesively bonded joints, World Congress on Computational Mechanics WCCM VII, LA, USA, 2006.

36. Blackman, B. R. K., Kinloch, A. J., Rodriguez Sanchez, S., Teo, W. S., Williams, J. G., The fracture behaviour of structural adhesives under high rates of testing, *Eng. Fract. Mech.* **76** (2009), 2868-2889.
37. Webb, T. W., Aifantis, E. C., Oscillatory fracture in polymeric materials, *Int. J. Solids Struct.*, **32** (1995), 2725-2743.
38. Macon, D. J., Anderson, G. L., Kinetic energy corrections for stick-slip behavior in brittle adhesives, *J. App. Polymer Sci.* **86** (2002), 1821-1828.
39. Maugis, P., Subcritical crack growth, surface energy, fracture toughness, stick-slip and embrittlement, *J. Mater. Sci*. **20** (1985), 3041-3073.
40. Rodriguez Sanchez, S., Fracture behaviour of automotive adhesive joints, PhD thesis, Imperial College London, 2008.
41. OpenFOAM, www.wikki.co.uk, www.openfoam.co.uk
42. Georgiou, I., The fracture of adhesively-bonded aluminium joints for automotive structures, PhD thesis, Imperial College London, 2003.
43. BS EN ISO 527:1996 Plastics - Determination of Tensile Properties.
44. ISO 25215:2009 - Determination of the mode I adhesive fracture energy G_{IC} of structural adhesives using the double cantilever beam (DCB) and tapered double cantilever beam (TDCB) specimens.
45. Vision Research, www.visionresearch.com
46. Kinloch, A. J., Williams, J. G., Crack blunting mechanisms in polymers. *J Mater. Sci.* **15** (1980), 987-996.
47. Blackman, B. R. K., Kinloch, A. J., Paraschi, M.,Teo, W. S., Measuring the mode I adhesive fracture energy, G_{Ic}, of structural adhesive joints: The results of an International round-robin. *Int. J. Adhesives &Adhesion* **23** (2003), 293-305.
48. Wang, Y., Williams, J. G., Dynamic crack growth in TDCB specimens. *Int. J Mech. Sci.* **38** (1996), 1073-1088.
49. Teo, W.S., The performance of adhesively bonded carbon-fibre composite joints: Pre-bond moisture and rate effects, PhD Thesis, Imperial College London, 2008.
50. Ivankovic, A., Finite volume modelling of dynamic fracture problems, *Computer Modelling and Simulation in Eng.* **4** (1999), 227-235.
51. Stylianou, V.,Ivankovic, A., Finite volume analysis of dynamic fracture phenomena, Part II: A Cohesive Zone Type Modelling, *Int. J. Fract.* **113** (2002), 125-151.
52. Rager, A., Williams, J. G.,Ivankovic, A., Numerical analysis of the three point bend impact tests for polymers, *Int. J. Fract.* **135** (2005), 201-217.
53. Murphy, N.,Ivankovic, A., The prediction of dynamic fracture evolution in PMMA using a cohesive zone model, *Eng. Fract. Mech.* **72** (2005), 861-875.
54. Murphy, N., M. Ali, Ivankovic, A., Dynamic crack bifurcation in PMMA, *Eng. Fract. Mech.* **73** (2006), 2569-2587.
55. Ivankovic, A., Venizelos, G. P., Rapid crack propagation: Predicting full-scale critical pressure from S4 test results, *Eng. Fract. Mech* **59** (1998), 607-622.
56. Greenshields, C. J., Venizelos, G. P., Ivankovic, A., A fluid/structure model for fast brittle fracture in pipes, *J. Fluids and Structures* **14** (2000), 221-234.
57. Ivankovic A., Tropsa V., Jasak H., Leevers P. S., Fully predictive model of RCP in plastic pipes, Proc. Plastic Pipes XI, Munich, 3-6 September, 2001.
58. Karac, A., Ivankovic, A., Behaviour of fluid filled PE containers under impact: Theoretical and numerical investigation. *Int. J. Impact Eng.* **36** (2009), 621-631.
59. A. P. Boresi, O. M. Sidebottom, Advanced Mechanics of materials, John Wiley & Sons, 1985 (Chapter 9).
60. Cooper, V., The fracture behaviour of nano-toughened structural epoxy adhesives, PhD Thesis, University College Dublin, 2010.

Table 1. Mechanical properties of AL EN AW 2014-A ([40]).

E_s [GPa]	σ_y [MPa]	*UTS*[MPa]	ρ_s[kg/m^3]	ν_s
72.4	430	485	2700	0.33

Table 2. Mechanical properties of XD4600adhesive at 23^{o}C as a function of rate ([40]).

Test speed [m/s]	Strain rate [s^{-1}]	0.2% σ_y [MPa]	E_a [GPa]	*UTS*[MPa]
0.00000017	2.27E-06	38.0	3.2	59.0
0.0000017	2.27E-05	40.2	3.4	62.0
0.000017	2.27E-04	43.5	3.4	61.0
0.00017	2.27E-03	47.4	3.8	70.0
0.0017	2.27E-02	51.1	4.1	74.0
0.1	1.33	53.6	4.6	88.0
1	13.33	55.1	4.8	89.0
5	66.67	54.9	4.9	90.0
8.3*	110.67	57.5	5.0	92.8
9.6*	128	57.6	5.0	93.0
13.5*	180	58.0	5.0	93.8

Note: * Obtained by linear extrapolation from measured data. These are required for numerical modelling of the TDCB tests.

Table 3: Fracture types and respective test and average crack velocity range.

Type of crack propagation		Test rate range [m/s]	Crack velocity range [m/s]
1	Slow-rate, stable	< 0.1 ±5%	< 2.5 ±10%
2	Slow-rate, stick-slip	(0.1 – 2.5) ±5%	(2.5 – 65) ±10%
3	High-rate, stick-slip	(2.5 – 6.0) ±5%	(65 – 150) ±10%
4	High-rate, stable	> 6.0 ±5%	> 150 ±10%

Table 4. Equations used for calculation of G_{Ic} for the TDCB specimens [36].

Analysis Type	Analysis Equations (Experimental data used)
'Type 1' Slow-rate stable	$G_{Ic} = G^{s}_{Ic} = \frac{4P^2 m}{E_s b^2}\left[1 + 0.43\left(\frac{3}{ma}\right)^{1/3}\right]$ (Crack propagation values used)
'Type 2' Slow-rate unstable	$G_{Ic} = G^{s}_{Ic} = \frac{4P^2 m}{E_s b^2}\left[1 + 0.43\left(\frac{3}{ma}\right)^{1/3}\right]$ (Crack initiation values used)
'Type 3' Fast-rate unstable	$G_{Ic} = \frac{E_s}{4m}\left(\frac{\delta}{2a^*}\right)^2\left[1 + 0.43\left(\frac{3}{ma}\right)^{1/3}\right]\left[1 - 3\left(\frac{9}{22}\right)^3\left(\frac{a^*}{C_L t}\right)^2 m \cdot h_s(a^*)\right]$ where $a^* = a + 0.64\left(\frac{3a^2}{m}\right)^{1/3} - \frac{2}{3}x_0$ and $C_L = \sqrt{E_s/\rho_s}$ (Crack initiation values used)
'Type 4' Fast-rate stable	$G_{Ic} = G^{s}_{Ic}\left\{1 - \frac{9}{11}\left(\frac{\dot{a}}{C_L}\right)^2\left[1 + 0.43\left(\frac{3}{ma}\right)^{1/3}\right]^2 m \cdot h_s(a^*)\right\}$ where $G^{s}_{Ic} = \frac{E_s}{4m}\left[\frac{(V/2)}{\dot{a}}\right]^2\left[1 + 0.43\left(\frac{3}{ma}\right)^{1/3}\right]^{-1}$ (Crack propagation values used)

Table 5: Mechanical properties of XD4600 adhesive for the FVM/CZM simulations.

TDCB test speed, m/s	Strain-rate at crack tip, 1/s		Adhesive properties		
	Analytical (DCB)	FVM simulations	E_a [GPa]	σ_y [MPa]	*UTS* [MPa]
3.3×10^{-6}	7.3e-05	5.0e-05	3.4	40.6	61.9
0.72	1.4e+01	1.0e+01	4.7	54.7	88.7
1.	1.9e+01	1.3e+01	4.8	55.0	89.1
2.5	4.7e+01	2.9e+01	4.8	55.0	89.3
5.	9.2e+01	6.0e+01	4.9	54.9	89.9
8.3	1.5e+02	1.1e+02	5.0	57.5	92.8
9.6	1.7e+02	1.2e+02	5.0	57.6	93.0
13.5	2.5e+02	1.8e+02	5.0	58.0	93.8

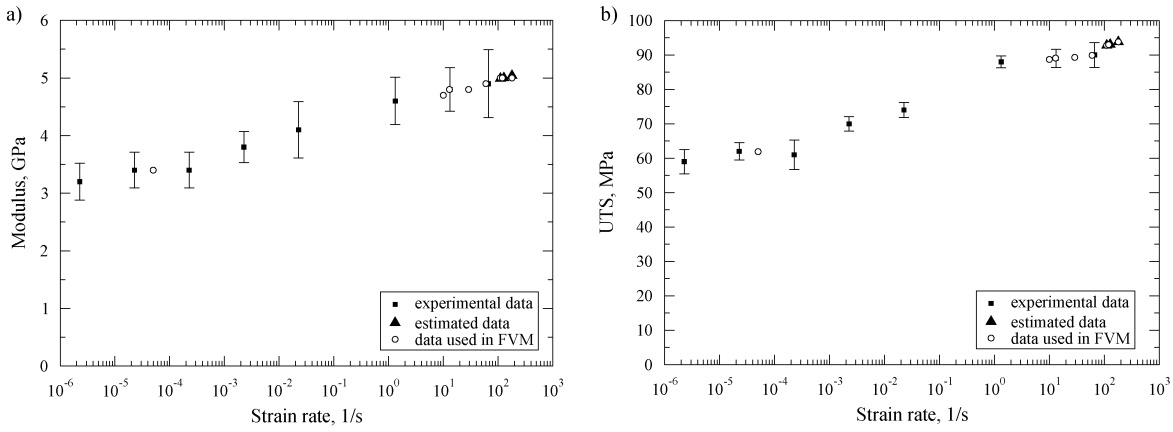

Figure 1: Mechanical properties of the adhesive as a function of strain rate;
(a) Young's modulus, (b) *UTS*.

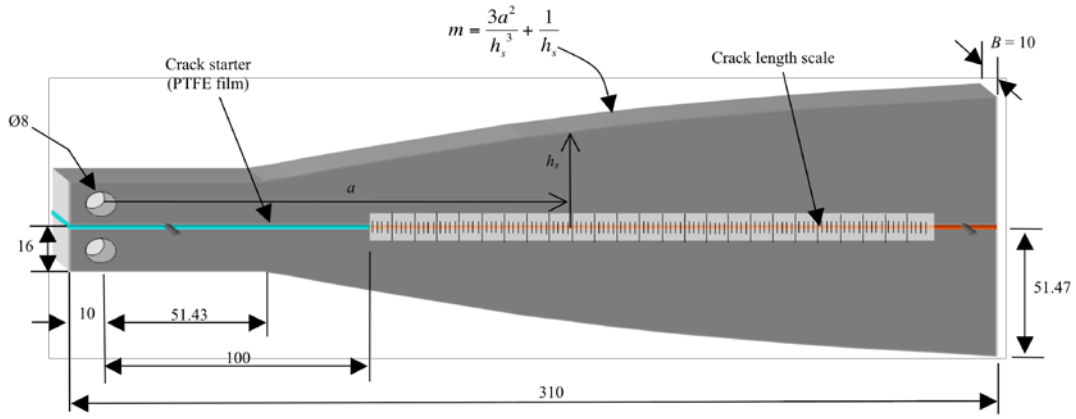

Figure 2: Schematic representation of a TDCB specimen (all dimensions in mm).

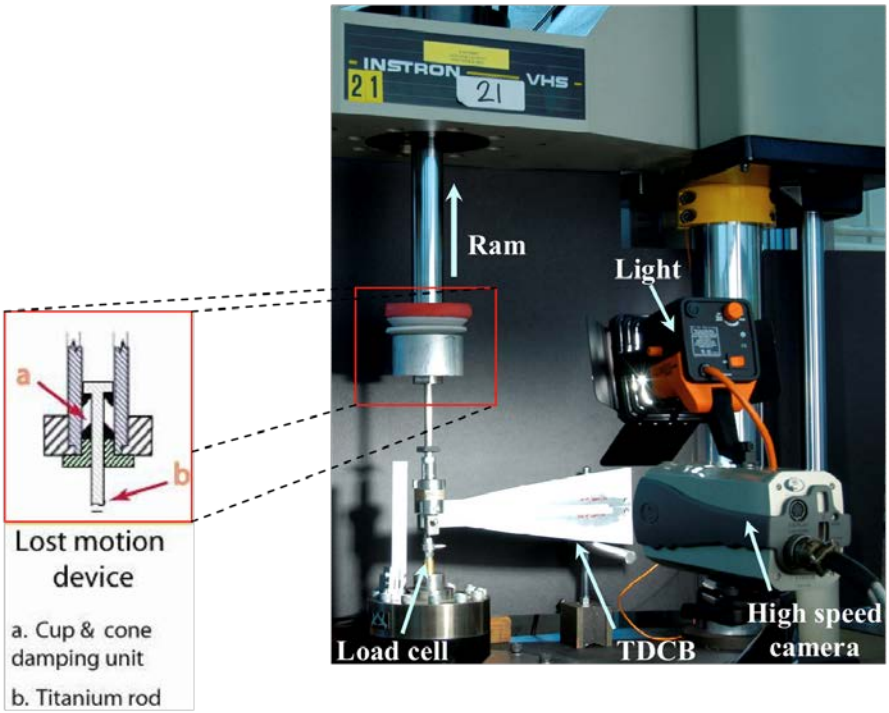

Figure 3: Test set-up for high-rate tests.

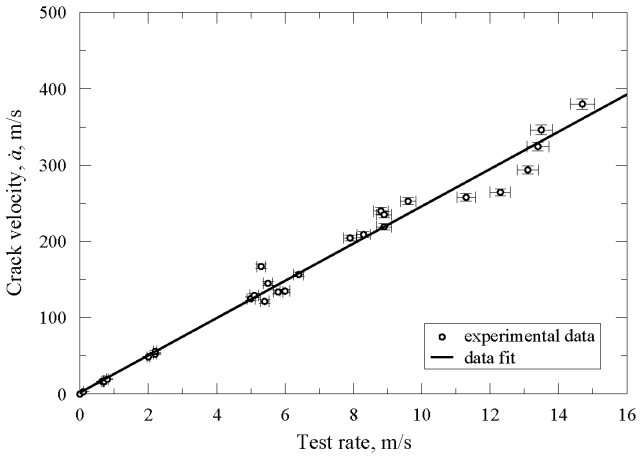

Figure 4: Average crack velocity versus rate of test.

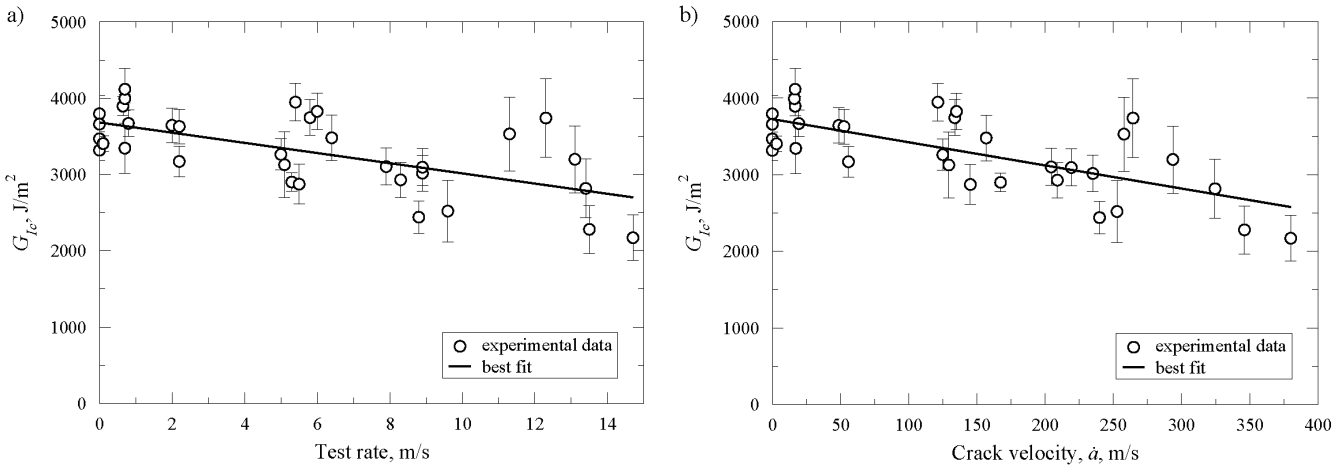

Figure 5: Adhesive fracture energy, G_{Ic}, as a function of: (a) rate of test, (b) average crack velocity [36].

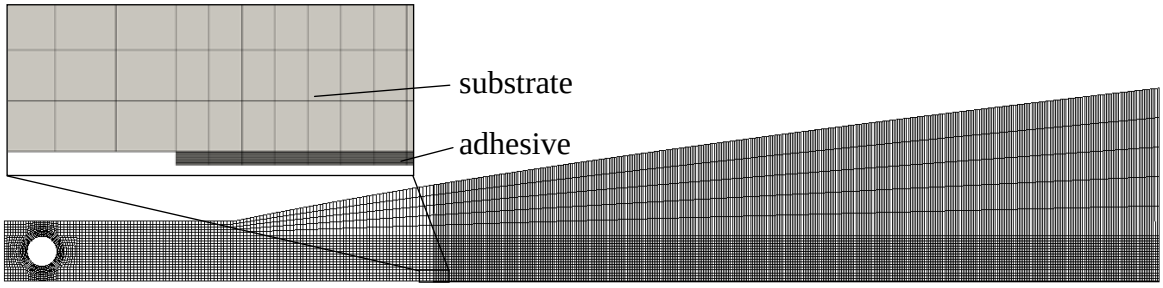

Figure 6: Typical FVM mesh of the TDCB specimen (quarter of the specimen modelled).

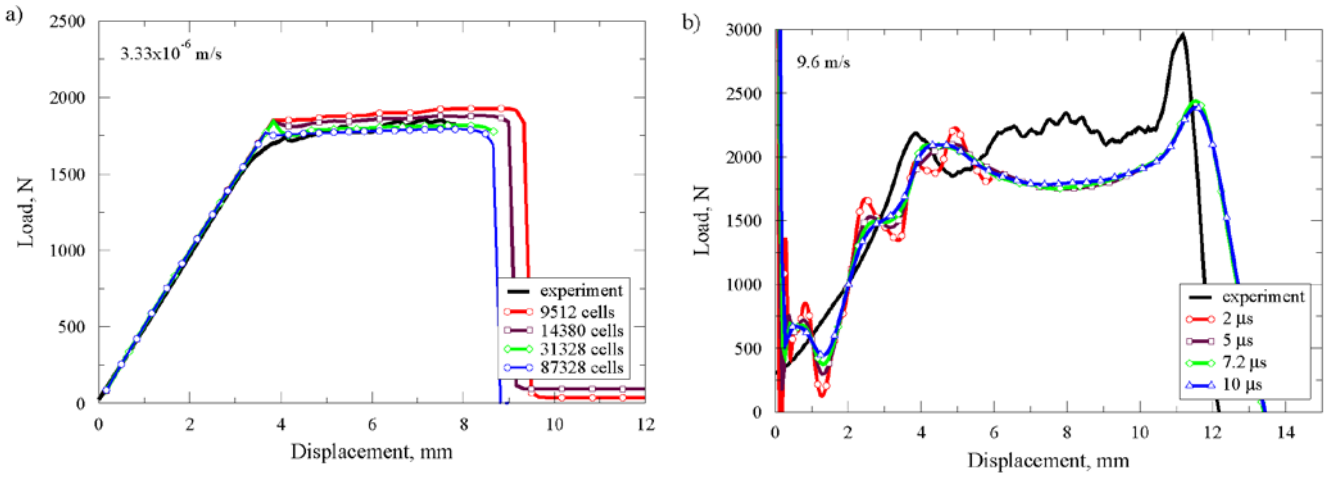

Figure 7: Sensitivity studies
(a) Mesh: 'Type 1' @ 3.33 x 10^{-6} m/s, E_a = 3.4 GPa, σ_y = 40.6 MPa, σ_{CZ} = 61.9 MPa, G_{Ic} = 3.6 kJ/m^2,
(b) Time: 'Type 4' @ 9.6 m/s, E_a = 5 GPa, σ_y = 57.6 MPa, σ_{CZ} = 93 MPa, G_{Ic} = 3.01 kJ/m^2.

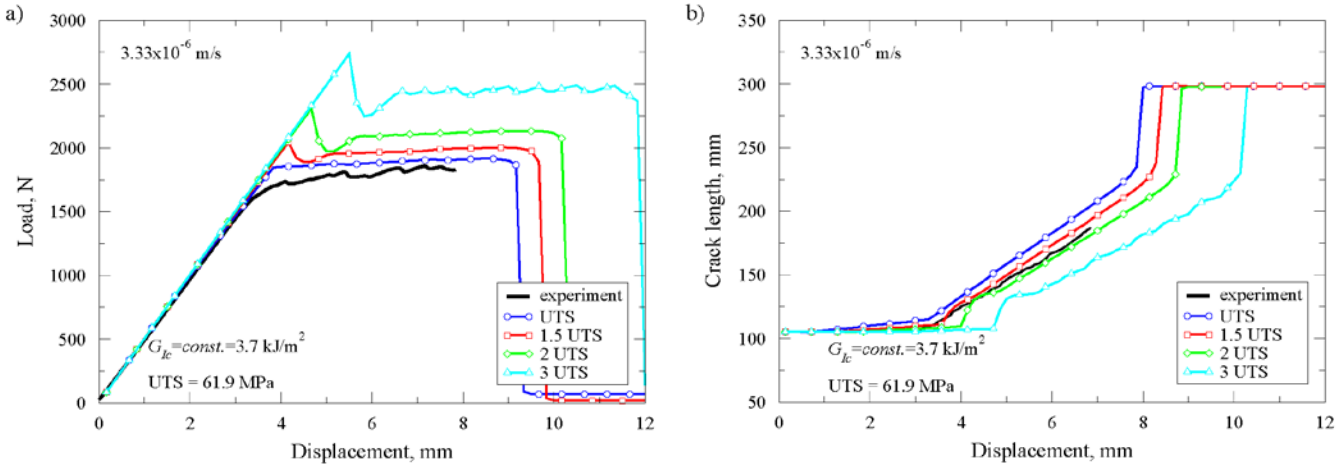

Figure 8: Using a rate-independent (i.e. constant) G_{Ic} value in the CZM and the effect of the value of the cohesive strength, σ_{CZ}, (i.e. the UTS) employed: 'Type 1' @ 3.33 x 10^{-6} m/s, E_a = 3.4 GPa, σ_y = 40.6 MPa, σ_{CZ}=61.9 MPa, G_{Ic} = 3.7 kJ/m^2.

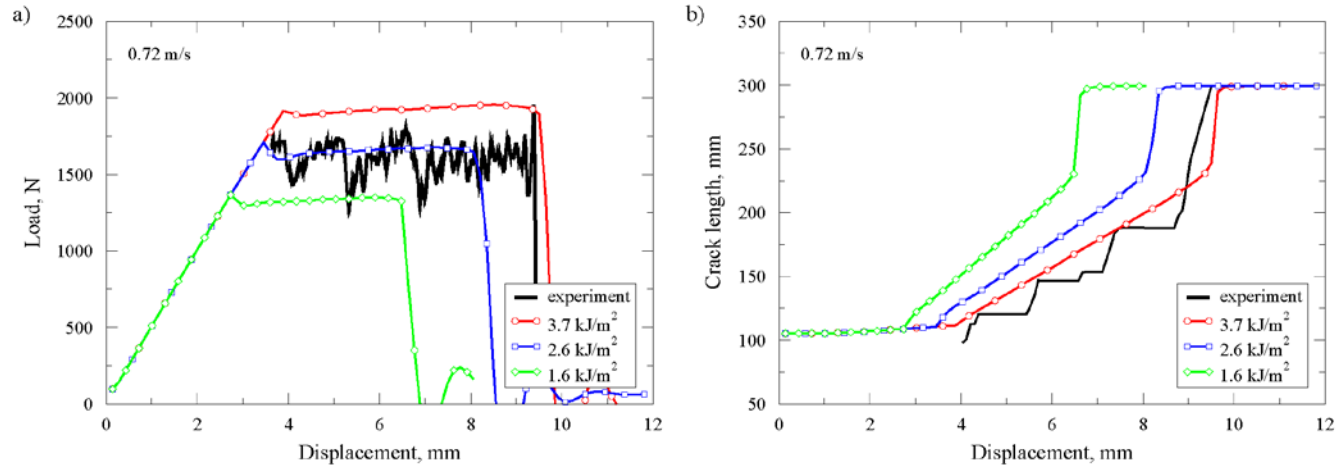

Figure 9: Using a rate-independent (i.e. constant) G_{Ic} value in the CZM and the effect of the constant G_{Ic} value: 'Type 2' @ 0.72 m/s, E_a = 4.7 GPa, σ_y = 54.7 MPa, σ_{CZ}=88.7 MPa.

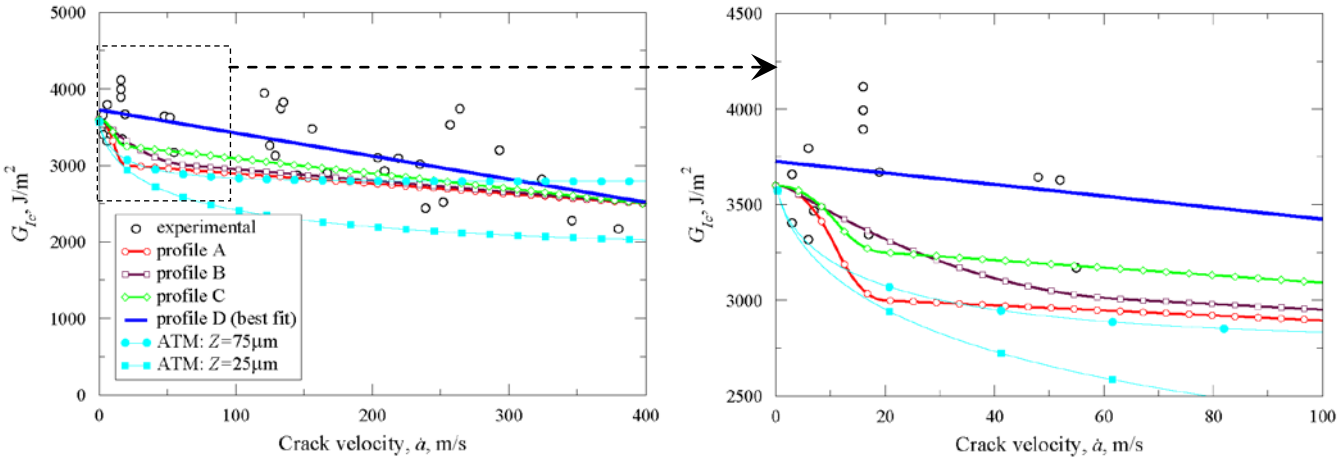

Figure 10: 'Profiles' of G_{Ic} versus average crack velocity used in the FVM/CZM numerical simulations when using a rate-dependent G_{Ic} value for the CZM.

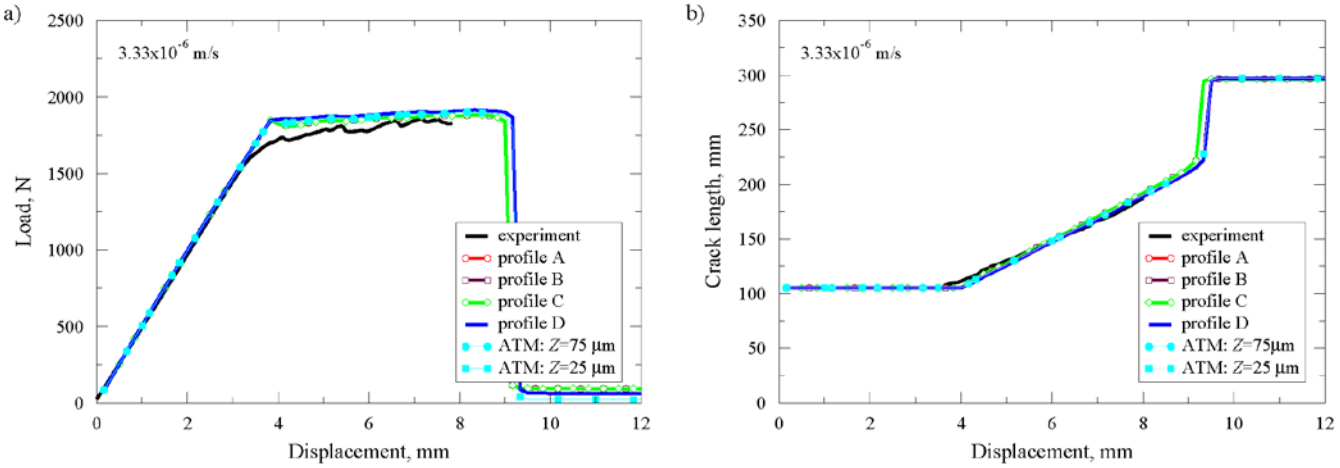

Figure 11: Rate-dependent G_{Ic} used in the CZM: 'Type 1' @ 3.33 x 10^{-6} m/s, E_a = 3.4 GPa, σ_y = 40.6 MPa, σ_{CZ} = 61.9 MPa.

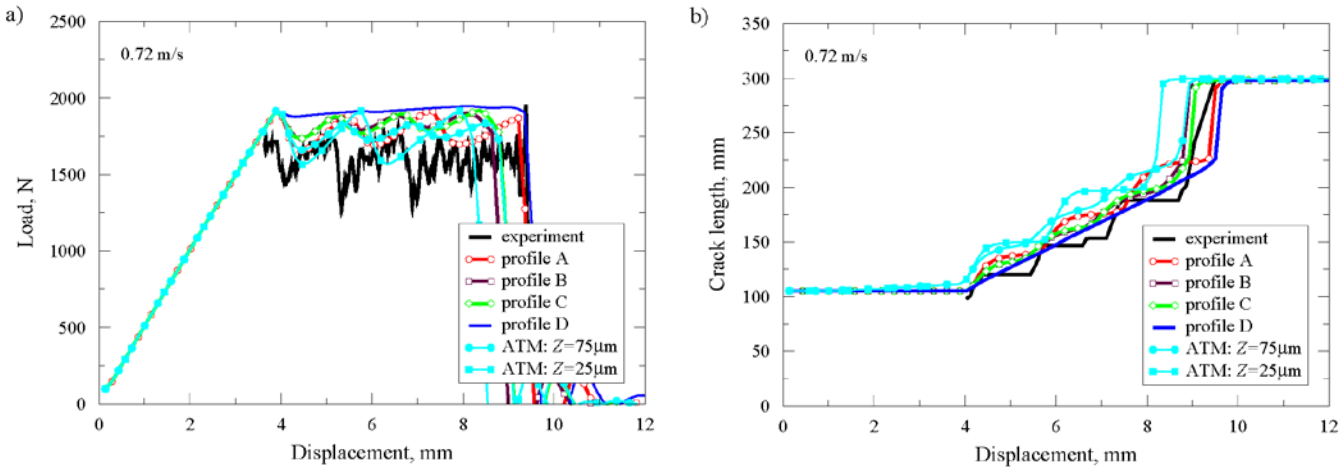

Figure 12: Rate-dependent G_{Ic} used in the CZM: 'Type 2' @0.72 m/s, E_a = 4.7 GPa, σ_y = 54.7 MPa, σ_{CZ} = 88.7 MPa.

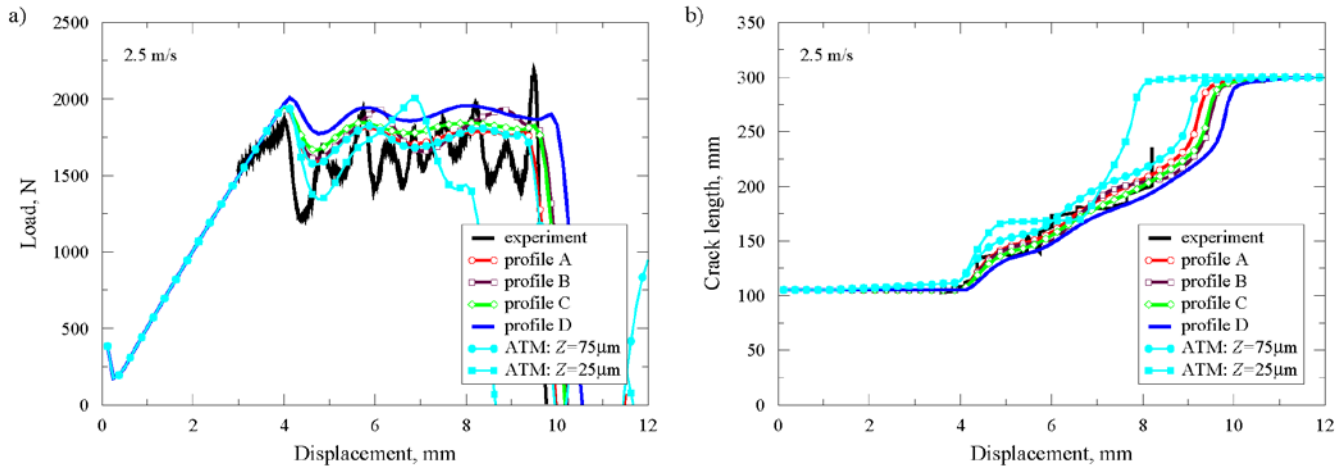

Figure 13: Rate-dependent G_{Ic} used in the CZM: 'Type 3' @ 2.5 m/s, E_a = 4.8 GPa, σ_y = 55 MPa, σ_{CZ} = 89.3 MPa.

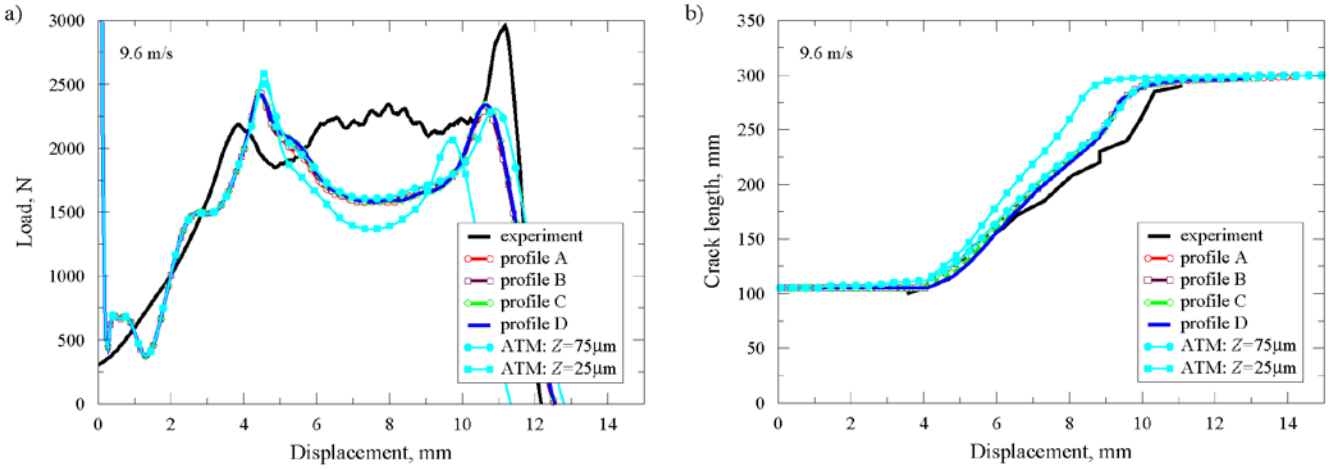

Figure 14: Rate-dependent G_{Ic} used in the CZM: 'Type 4' @ 9.6 m/s, E_a = 5.0 GPa, σ_y = 57.6 MPa, σ_{CZ} = 93.0 MPa.

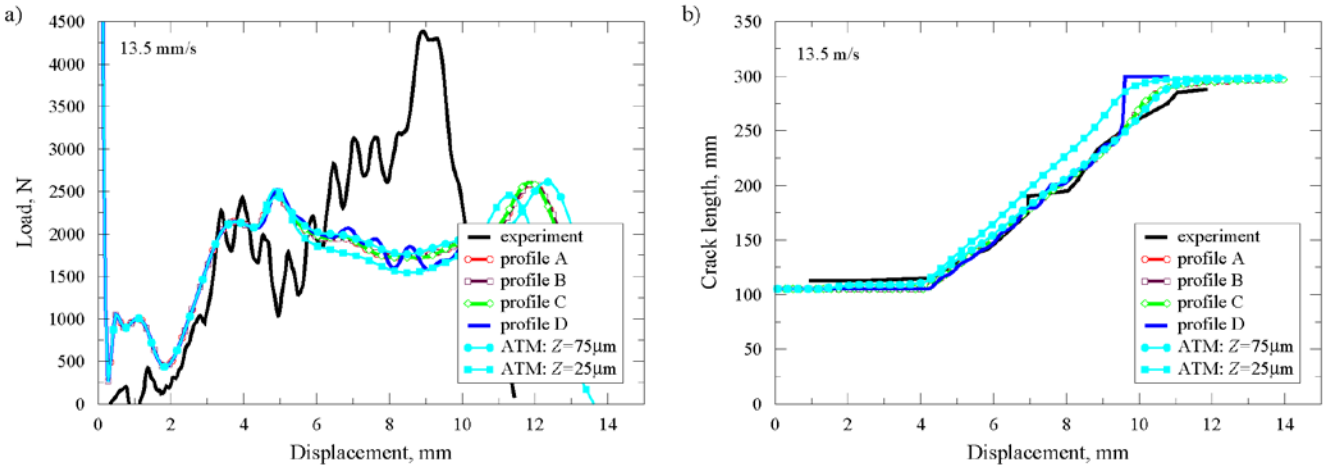

Figure 15: Rate-dependent G_{Ic} used in the CZM: 'Type 4' @ 13.5 m/s, E_a = 5.0 GPa, σ_y = 58 MPa, σ_{CZ} = 93.8 MPa.

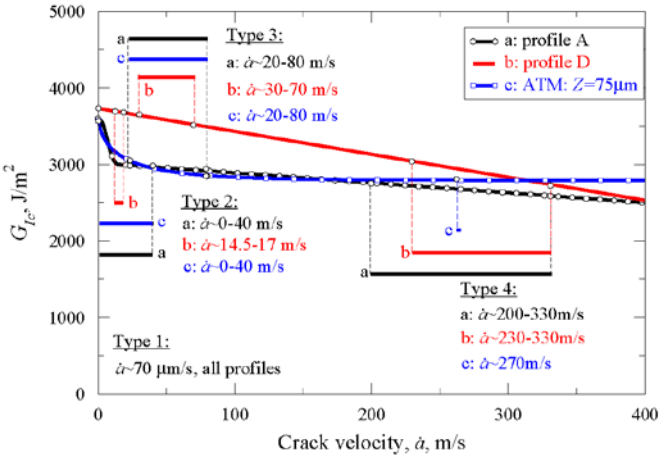

Figure 16: Predicted variations of crack velocity with G_{Ic} for the various fracture types when 'Profiles A, D and ATM=75 µm' are used in the CZM for the FVM/CZM numerical simulations.

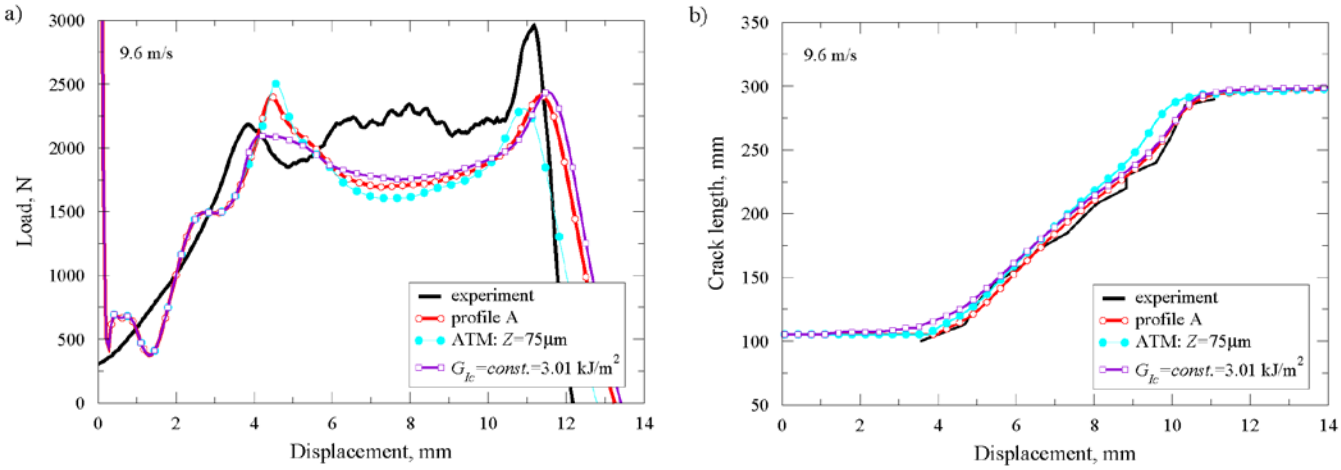

Figure 17: Effect of using a rate-dependent G_{Ic} value (i.e. 'Profiles A and ATM=75 µm') versus a rate-independent (i.e. constant) G_{Ic} value for the CZM in the FVM simulations, also showing a comparison to the experimental data: 'Type 4' @ 9.6 m/s, E_a = 5.0 GPa, σ_y = 57.6 MPa, σ_{CZ} = 93.0 MPa.